JGR Oceans

RESEARCH ARTICLE
10.1029/2020JC016367

Special Section:
Coastal hydrology and oceanography

Spatial Footprints of Storm Surges Along the Global Coastlines

Alejandra R. Enríquez[1], Thomas Wahl[1], Marta Marcos[2,3], and Ivan D. Haigh[4]

[1]Department of Civil, Environmental and Construction Engineering & National Center for Integrated Coastal Research, University of Central Florida, Orlando, FL, USA, [2]Department of Physics, University of the Balearic Islands, Palma, Spain, [3]IMEDEA (UIB-CSIC), Palma, Spain, [4]School of Ocean and Earth Science, National Oceanography Centre, University of Southampton, Southampton, UK

Key Points:
- Contiguous and unconnected coastal stretches are often affected by the same storm surge event.
- Storm surge reanalysis data is able to correctly represent the spatial patterns of storm surge.
- A set of reference storm surge time series can be used as indicators of storm surge behavior for spatially coherent coastlines.

Supporting Information:
- Supporting Information S1

Correspondence to:
A. R. Enríquez,
a.enriquez@ucf.edu

Citation:
Enríquez, A. R., Wahl, T., Marcos, M., & Haigh, I. D. (2020). Spatial footprints of storm surges along the global coastlines. *Journal of Geophysical Research: Oceans*, *125*, e2020JC016367. https://doi.org/10.1029/2020JC016367

Received 4 MAY 2020
Accepted 18 AUG 2020
Accepted article online 25 AUG 2020

Abstract We perform the first global analysis of the spatial footprints of storm surges, using observed and simulated storm surge data. Three different techniques are applied to quantify the spatial footprints: clustering analysis, percentage of co-occurrence, and joint probability analysis. The capability of the simulated data to represent the observed storm surge footprints is demonstrated. Results lead to the identification of coastline stretches prone to be impacted simultaneously by the same storm surge events. The spatial footprint sizes differ around the globe, partially conditioned by the geography of the coastline, that is, more irregular coastlines consist of a larger number of different storm surge clusters with varying footprint sizes. For the northwestern Atlantic, spatial footprints of storm surges vary when specifically accounting for tropical cyclones, using storm track information in the storm surge simulations. Our results provide important new insights into the spatial footprints of storm surges at the global scale and will help to facilitate improvements in how coastal flood risk is identified, assessed, and managed, by taking these spatial features into account.

Plain Language Summary When an extreme storm surge event impacts a particular site on the coast, other coastal locations are expected to also experience an extreme storm surge. Thus, a single extreme event can affect multiple critical service locations, populations, interconnected infrastructure systems, and diverse industrial sectors simultaneously, increasing the impact level of the event. Understanding the spatial dependence of surges on coasts is crucial for accurate risk analyses and the development of efficient emergency management plans. In the present paper, we identified the coastal stretches prone to be impacted simultaneously by a storm surge event. Our results show that not only contiguous but also unconnected coastlines are often affected by the same storm surge events and highlight that the spatial footprints of storm surges are not biased toward individual extreme events. Instead, we find that many other events, smaller in height and intensity (while still being extremes), have similar spatial footprints.

1. Introduction

Flooding is among the most dangerous natural hazards for urban settlements along the global coastline (Needham et al., 2015). A high proportion of the world's population, approximately 10%, live in the Low Elevation Coastal Zone (land below 10-m height from mean sea level), and there is an ongoing trend of migration toward the coast (McGranahan et al., 2007). In this context, it has been estimated that one third of the global coastal population (189.2 million) was exposed to a 1 in 100-year water level in the Year 2000 (Neumann et al., 2015). According to Hallegatte et al. (2013), the average losses due to coastal flooding across the 136 largest port cities were estimated to be approximately US$6 billion in 2005. Without adaptation measures, the impacts of coastal flooding are expected to increase in the future. Among all coastal flooding drivers (tsunamis, extreme precipitation, high river discharge, storm surge, extreme waves, and/or a combination of these elements), storm surges are the deadliest hazard at coasts (Von Storch & Woth, 2008).

The relevance of flooding for coastal regions has driven research to improved understanding of extreme sea levels and storm surges from many different perspectives. Overall, the related literature has focused on extreme sea level and storm surge intensity, variability, long-term trends, uncertainties in the estimates, its correlation with climate modes, and their interaction with other ocean parameters such as tides, mean sea level, or waves (Marcos & Woodworth, 2017; Mawdsley et al., 2015; Von Storch & Woth, 2008;

Vousdoukas et al., 2018; Wahl et al., 2012, 2017; Wahl & Chambers, 2015, 2016). Less attention has been paid to the study of the spatial extension of storm surges, that is, the simultaneous exceedance of critical thresholds over a certain distance caused by a single storm surge event, here termed as "spatial footprint." However, understanding the spatial footprints of storm surges on coasts is highly relevant to derive effective risk management and protection plans, since the impact of storm surges may be aggravated as a result of the simultaneous economic and personal damages and losses along a stretch of coastline. A recent example was Hurricane Dorian (September 2019), which caused extreme storm surges along many thousands of kilometers of the coasts of Abaco and Grand Bahama Islands and the southeastern United States, including the states of Florida, Georgia, South Carolina, and North Carolina (NWS, 2019a, 2019b).

The spatial footprints of storm surges have been previously studied for specific extreme events, particularly focused on tropical and extratropical cyclones (Dullaart et al., 2020; Hope et al., 2013; Mattocks & Forbes, 2008; Muis et al., 2019; Rego & Li, 2010; Westerink et al., 2008). However, only two studies have comprehensively assessed the spatial coherence of extreme sea levels and surges on coasts so far (Haigh et al., 2016; Stephens et al., 2020). Through an event-analysis method, they studied the spatial patterns of extreme sea levels and skew surges along the United Kingdom and New Zealand coasts, respectively, by using tide gauge measurements. These studies have provided insights into the spatial footprints of storm surges but were focused on specific study areas and were limited by the availability of long time series of observed sea level.

The relevance of accounting for spatial dependences of natural hazards has been demonstrated, in particular for river floods (Berghuijs et al., 2019; Jongman et al., 2014; Keef et al., 2009; Quinn et al., 2019; Villarini et al., 2011). Jongman et al. (2014) found that the potential economic losses of river floods are underestimated if the spatial dependencies of extreme river discharge events are neglected. Furthermore, flood impacts lead to a cascading of direct and indirect economic losses because of impacts to multiple economic sectors simultaneously as well as along supply chains (Willner et al., 2018). Therefore, reliable information on correlated loss probabilities is crucial for developing robust risk management plans. Despite its importance, few studies included the spatial correlation of storm surges on coasts, where at-site univariate return periods are typically used in broad-scale risk assessments. One notable exception is the work of Vousdoukas et al. (2020), who included the spatial dependences of extreme sea levels in their cost-benefit analysis of raising dikes in Europe to mitigate flood risk during the 21st century.

The main aim of this paper is to assess the spatial patterns of storm surges for the global coastline by using high-resolution reanalysis surge data. The use of simulated data, from Muis et al. (2016), allows us to understand the spatial coherence of storm surges around the world's coastline, regardless of the availability of observed sea level data, which usually limits coastal hazards assessments, particularly in the southern hemisphere (Church & White, 2006). Where possible, the capability of the reanalysis data to reproduce the spatial footprints of storm surges is validated against observations. In addition, an updated storm surge reanalysis data set, which specifically accounts for tropical cyclone storm track information, is used to assess the storm surge footprints along the northwestern Atlantic coast. Three different methods are applied to both reanalysis and observations to examine the spatial footprints of storm surges: K-Means clustering algorithm, match level analysis, and copula analysis. K-Means clustering algorithm (Hastie et al., 2009) is used to classify the storm surge data into different groups according to the similarity among storm surge time series. Then, K-Means results are used to assess the match levels and joint return periods (through the copula analysis) across locations.

2. Data

We use two types of storm surge data here: (1) reanalysis and (2) observations from tide gauges. Storm surge reanalysis data are retrieved from the Global Tide and Surge Reanalysis (GTSR) data set of Muis et al. (2016). Storm surges were simulated by using the Global Tide and Surge Model forced with surface wind speed and atmospheric pressure from the ERA-Interim global atmospheric reanalysis. Extreme sea level and storm surge outputs are available along the world's coastline at 16,395 locations matching the centroids of the segments in the Dynamic Interactive Vulnerability Assessment model (Vafeidis et al., 2008) database. The GTSR data have high temporal resolution (every 10 min from 1979 to 2014), but for our analysis, we only use daily maxima surge values.

GTSR time series were previously validated site-by-site (in terms of surge height) with observations at tide gauge locations, showing good agreement between observed and simulated storm surge heights (Muis et al., 2016). However, extreme storm surges were found to be underpredicted, particularly in regions affected by tropical cyclones, as one would expect given the low resolution of the meteorological forcing used. Thus, Muis et al. (2019) developed an updated storm surge and extreme sea level reanalysis for the northwestern Atlantic coasts, for the period 1988 to 2015, which explicitly accounts for tropical and extratropical cyclones. This updated reanalysis was obtained by forcing the Global Tide and Surge Model with EBTRCK and ERA-Interim wind and pressure fields. Here, the spatial footprints of storm surges along the northwestern Atlantic coast are assessed by using both the global and the updated (regional) version of GTSR.

Observed storm surge time series are used for validation and obtained from the tide gauge sea level records, compiled in the updated Global Extreme Sea Level Analysis Version 2 database (Woodworth et al., 2016). This data set is composed of 1,355 tide gauge records distributed worldwide with hourly (or higher) temporal sampling. However, some of these sea level records correspond to the same stations due to the existence of different data providers and due to different instruments covering different periods of time. In this study, the observed data set is restricted to have only one sea level record for each station. In addition, in order to have sea level time series with similar lengths, the observed data are constrained to tide gauges operating between 1960 and 2014, covering at least 70% of this period and located in one of the study areas (study areas are described in section 4). This reduces the number of records to 300 sites.

Daily maxima of observed storm surges are computed from sea level records following previous studies (Haigh et al., 2016; Marcos & Woodworth, 2017). First, sea level time series are linearly detrended, so the magnitude of events are directly comparable over the whole period, regardless of mean sea level changes. Second, the astronomical tide is removed from the total sea level observations, to leave the nontidal residual, which primarily contains the storm surge component. The astronomical tide is calculated using the t-tide Matlab® toolbox at each of the 300 tide gauge sites for each calendar year and using 67 tidal constituents. In addition to the daily maxima, the extreme storm surges are identified, for both observed and reanalysis data, by applying a peaks-over-threshold method using a 95th percentile threshold at each location. The analysis is repeated using the 99th percentile threshold for two regions (see supporting information Figures S37–S40) to assess sensitivity of the results to the threshold selection. To ensure independence, a declustering algorithm using a 3-day window is imposed.

3. Methods

We apply three methods to obtain the spatial footprints of storm surges, namely, (1) K-Means clustering algorithm, (2) match level analysis, and (3) copula analysis. First, K-Means is used for an initial clustering of storm surges along the coastline as well as the identification storm surge time series corresponding to the center of masses of each group, the cluster centers. Here, the storm surge series corresponding to the cluster centers are considered representative of each cluster and referred to as "reference series" hereafter (further information can be found in section 4.1). By using the reference series, the match level and copula analyses are performed to obtain the spatial footprints in terms of co-occurrences and joint return periods. Note that the spatial footprints obtained by these two methods are not directly comparable.

After a set of sensitivity tests performed with the K-Means clustering algorithm, the spatial footprints of storm surges are studied separately for 10 regions (also shown in Figure S1), namely, (1) northeastern Pacific, (2) southeastern Pacific, (3) northwestern Atlantic, (4) southwestern Atlantic, (5) northeastern Atlantic, (6) southeastern Atlantic, (7) Indian Ocean, (8) Oceania (including in this region the Banda Sea and surroundings), (9) northwestern Pacific, and (10) South China Sea (including in this region the coastline from Indonesia/Molucca Sea up to northern Philippines). The comparison between the footprints obtained by using reanalysis and observed storm surge data is performed only in five of these regions, where enough observations are available, namely, (1) northeastern Pacific, (3) northwestern Atlantic, (5) northeastern Atlantic, (8) Oceania, and (9) northwestern Pacific.

For validation, we compare the clustering obtained from reanalysis data against the clustering obtained from observations for the three methods. The three methods and the validation process are described in detail in the following sections.

3.1. K-Means

The K-Means algorithm (Hastie et al., 2009) clusters a group of data into subgroups according to the degree of similarity between the objects being clustered. K-Means clustering starts an iteration process with random initialization of the positions of the cluster centers in the data space and then identifies the closest cluster center for each data point. Pearson's correlation is used to quantify similarity between storm surge time series and cluster centers, while the final clustering configuration (the position of the cluster centers) is based on the minimum of total cluster variance for a given cluster. As mentioned above, the storm surge series corresponding to the cluster centers are the "reference series" of each cluster. The reference series are, by construction, the time series showing the highest similarity with all other storm surge time series within a given cluster. Note that these reference series do not necessarily have to be located in the center of the cluster space from a geographic perspective.

Here, the K-Means algorithm is applied to the time series of extreme surge events (i.e., declustered events above the 95th percentile threshold; see section 3), and 50 random initializations are used. Note that the number of clusters (*NoC*) has to be stated before the iteration process starts. In order to find the *NoC* that best represents the spatial footprints of storm surges in each region, different values ranging from 5 to 20 are tested when using reanalysis data and from 2 to 10 when using observations. Setting the upper limit of *NoC* to 20 avoids local-scale footprints to become important. On the other hand, due to the low number of tide gauges available in the different regions (Figure S1), the variability of the observed storm surge time series has prompted restricting the upper limit of *NoC* to 10. The average correlation and average standard deviation are calculated for each of the clustering schemes obtained by using different *NoC*. The optimal *NoC* for each study area is selected based on the highest ratio of correlation to standard deviation.

3.2. Match Level

Although the K-Means algorithm assigns each storm surge time series to a respective group according to their correlation, the level of similarity among the different storm surge time series remains unknown. Therefore, we also perform a "match level" analysis: Matches are defined as extreme events (see section 3 for definition of "extreme") that occur simultaneously at two different coastal points within a 3-day time window. The match level is then expressed as a percentage of match. For the sake of simplicity, the match level is only calculated between the reference series of each cluster (derived from the K-Means algorithm) and all other storm surge time series, irrespective of the previous clustering boundaries.

3.3. Copula Analysis

The third approach we apply quantifies the probabilities of simultaneous exceedances of a prescribed return level across tide gauges or model grid points. We compute the probability that the reference series and each of the other storm surge time series simultaneously exceed their respective 10-year return level (probabilities of simultaneous exceedances of 50-year return level are also included for two regions in the supporting information). To do so, the joint return period is calculated between two time series (one is always the reference series, and the second one loops through all other time series) using a bivariate copula function. While the reference series are composed of the extreme storm surge events, all other time series comprise the complete storm surge time series (daily maxima; see section 2). We match the length of the two time series by taking the highest value of the daily maxima storm surge time series for each extreme event of the reference series, allowing for a 3-day time window lag.

The dependence between the two time series is quantified using Kendall's rank correlation: Only pairs with correlations higher than 0.15 are retained for the analysis, in agreement with previous works (Wahl et al., 2015). In order to facilitate direct comparison of the results, only one type of copula function is considered. After testing several options, the Gumbel copula was found to be the most appropriate based on goodness-of-fit testing, when compared to the other Archimedean copulas (Clayton and Frank). Joint return periods are calculated for the AND case assuming the respective 10-year level is exceeded simultaneously at both locations (Salvadori & De Michele, 2004).

Separately, the univariate 10-year return levels are calculated for the reference series following Muis et al. (2019): The univariate return levels are obtained by using the extreme storm surges above a threshold that is exceeded on average three times per year. To ensure independence, a declustering algorithm using a

Table 1
Optimal Number of Clusters (NoC) Resulting From Using Observations (Second Column) and Reanalysis (Third Column)

Study area	*NoC* using observations	*NoC* using the restricted reanalysis	*NoC* using the complete reanalysis
Northeastern Atlantic	6	10	18
Northwestern Atlantic	7	10	13
Northeastern Pacific	5	10	18
Oceania	6	9	9
Southeastern Atlantic			11
Indian Ocean			19
Southeastern Pacific			7
South China Sea			14
Southwestern Atlantic			19
Northwestern Pacific	5	6	20

3-day window is imposed. The univariate 50-year return levels for two regions are included in Figures S33 and S34.

3.4. Validation

Before performing the spatial footprint analysis using the complete reanalysis data set, the model's ability to reproduce the spatial footprints is validated. In addition, the clustering compositions resulting from the three different techniques (K-Means, match level, and copula analysis) are compared to assess sensitivity of the results to employing different methods. To ease the comparison among methods, match level results are assembled into a clustering map, so the results can be directly compared with K-Means. The clustering is performed by assigning each storm surge series to the reference series to which it shows the highest match. Similarly, the joint return period results are also presented as clusters, by grouping the storm surge series into the cluster for which the joint return period with the reference series is the lowest.

For consistency and in order to avoid discrepancies resulting from the higher spatial resolution of the reanalysis data set in comparison to the observed data, we select only reanalysis data points located at or near to the tide gauge sites. Then, the spatial footprints obtained by using this restricted reanalysis data set are compared with the footprints obtained from observations in areas with enough measurements: northeastern Atlantic, northwestern Atlantic, northeastern Pacific, Oceania, and northwestern Pacific.

The capability of the simulated data to reproduce the spatial footprints is validated in two different stages. The first one consists in a comparison of the optimal *NoC* obtained by using storm surge observations and the restricted reanalysis data set. In the second one, we contrast the extensions of the spatial footprints as well as the locations of the reference gauges between the two data sets. In this latter case, the optimal *NoC* is calculated using storm surge observations and then the same *NoC* is imposed on the restricted reanalysis data set to allow direct comparison of the results.

4. Results

4.1. Validation

The final *NoC* values for each region in the validation process are shown in the first (using observations) and second (using the restricted reanalysis data set) columns of Table 1. There is a disagreement between the optimal *NoC* obtained by using the two data sets, with a notable increase in the optimal *NoC* when using the restricted reanalysis in comparison with the observations.

Match level and joint return period results are displayed as clusters for direct comparison (see section 4). The clusters derived from using the two data sets (assuming the same *NoC* now) and the three methods are shown in Figure 1. There is overall good agreement between the clusters derived from observed and modeled storm surge data, although the reference series do not always coincide. A noteworthy example is the Oceania region, where the position of the reference series identified with K-Means changes from New Zealand (when using observations) to northwestern Australia (when using reanalysis data). Other changes, although smaller in terms of spatial shifts of reference sites, are found in the Caribbean Sea and northwestern Pacific coasts.

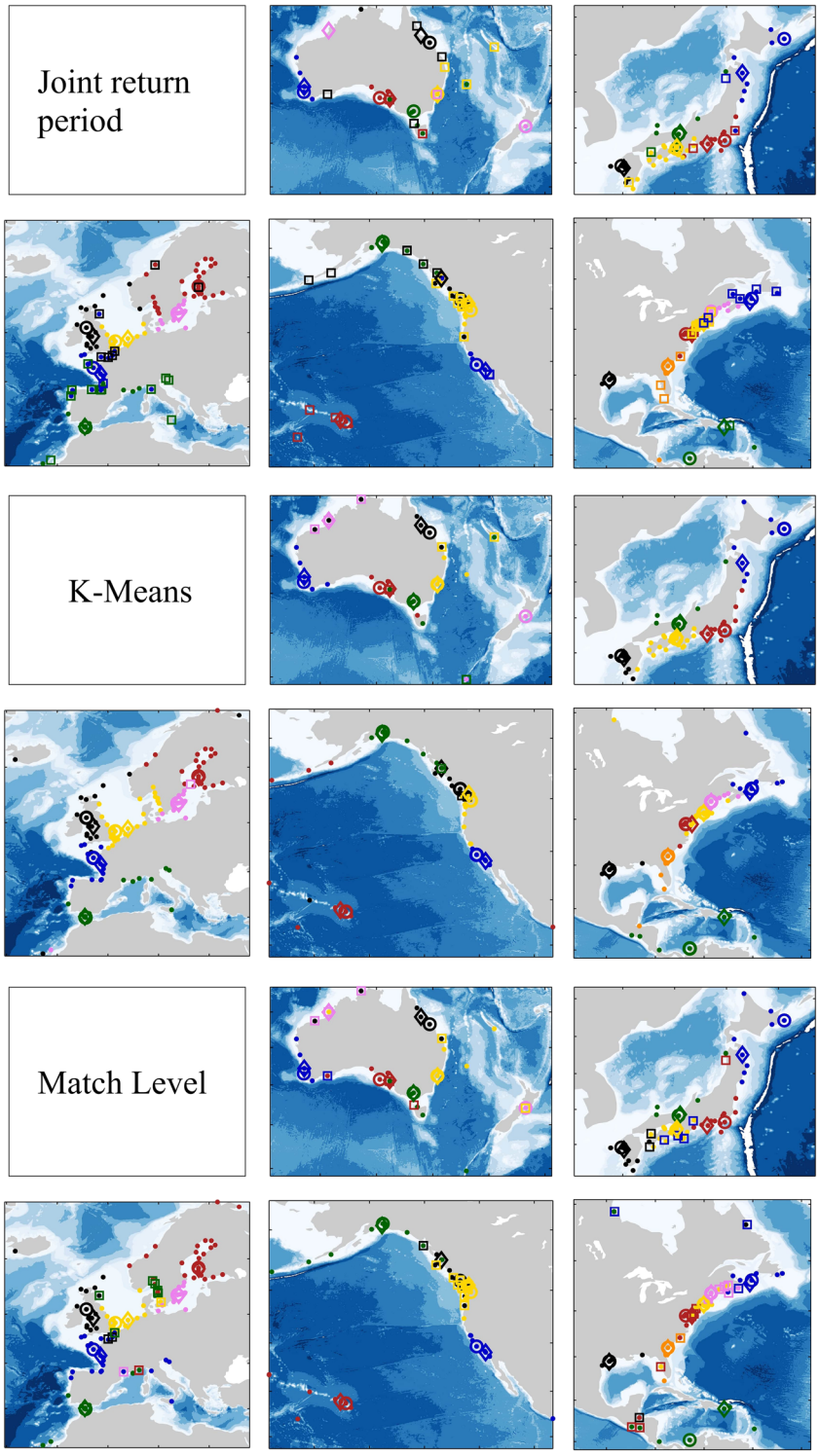

Figure 1. Comparison of the spatial footprints of storm surges obtained from using three different techniques (top, K-Means; middle, match level; bottom, copula analysis) and two data sets (observations and reanalysis). Reference series identified with the K-Means clustering are indicated by open circles (for observations) and diamonds (for reanalysis). Colored dots indicate overlap between the spatial footprints derived with the two data sets, whereas open squares indicate that these locations were assigned to a different cluster when using reanalysis data (the color indicates the cluster the location is assigned to).

Table 2
Validation Results

S1		Obs.		S2		Restr. Rean.		S3		Restr. Rean.	
Obs.		M.L.	C.	Restr. Rean.		M.L.	C.	Obs.		K-M	M.L.	C.
	K-M	83.3	63.3		K-M	88.3	71		K-M	80		
	M.L.		64.6		M.L.		69.3		M.L.		78.6	
									C.			62.3

Note. The clustering results obtained by using observations (Obs.) and the restricted reanalysis data (Restr. Rean.) are compared across different clustering methods (see S1 and S2 in Table 1; K-Means [K-M], match level [M.L.], and copula analysis [C.]) and across the two data sets (see S3 in Table 1). Copula results are AND joint return periods for univariate 10-year level exceedances.

Similarly, the clusters resulting from using the three methods are similar in most regions. Visible discrepancies are found in the Mediterranean Sea and Central American coasts, possibly due to the sparse number of tide gauges spread over large areas. As a consequence, some storm surge time series from different clusters have similar connections with more than one reference series. A marked case of mismatch is the cluster along northwestern Atlantic coasts (from Boston to Nova Scotia; Figure 1) where the cluster size is reduced when applying the match level method to the observations but is similar for the other two methods.

In addition to the visual comparison, the consistency of the clusters is also quantified as the percentage of storm surge time series found in the same cluster (percentage of agreement) across methods and data sets, confirming the overall good agreement (Table 2). Table 2 is divided in three sections: The first two sections show the percentage of agreement among methods (K-Means, match level, and copula analysis) when using observations only and restricted reanalysis only. The third section depicts the percentage of agreement between the two data sets for the three methods. Larger differences obtained with the copula analysis (compared to the other methods) are likely linked to the smaller number of time series used in this approach (since only pairs of storm surge time series with correlations higher than 0.15 are considered).

4.2. Spatial Footprints of Storm Surges

Having validated the hydrodynamic numerical model's skill in reproducing the spatial footprints of storm surges, as well as assessing robustness of results across the three methods, we now use the complete reanalysis data set to study the spatial footprints of storm surges along the global coastlines in more depth. The optimal *NoC* for each study area is recalculated since the higher resolution of the full reanalysis data set allows for obtaining a larger number of clusters within each region and, thus, finding possible unobserved spatial patterns. As a consequence, the positions of the reference series also change by using the full reanalysis data set. Results of K-Means clustering for the 10 regions can be found in Figures S2 to S11.

The final *NoC* values are listed in the third column of Table 1. Overall, the number of clusters notably increases in contrast to those obtained when using point-wise observations. A clear example is found along the northeastern Pacific coasts (going from five clusters using tide gauges to 18 using the full reanalysis data). However, clusters in some of the study areas remain unchanged. For instance, the Oceania coasts are represented by clusters covering almost the same areas as when using tide gauge observations, with the exception of the southernmost cluster that is merged with the one located in the Great Australian Bight (Figure S2). The Atlantic coasts of the United States and Canada show similar clustering under both observations and the complete reanalysis data (Figure S3), which is not surprising as these regions have dense tide gauge networks (Figure S1).

For the sake of simplicity, the spatial footprints of storm surges are shown only for the Oceania and northwestern Atlantic coasts obtained by using events over the 95th percentile threshold in Figures 2 to 5. Results for the other regions can be found in Figures S12 to S27 and spatial footprints obtained by using events over the 99th percentile threshold for the Oceania and northwestern Atlantic regions in Figures S37 to S40. The lengths of the coastline stretches where storm surges are correlated vary around the globe. Areas characterized by irregular coastlines (i.e., coastlines presenting a high variability of orientations) show a larger number of clusters; this is the case for the Mediterranean Sea and northern European coasts (Figure S6), northwestern Pacific coasts (Figure S5), and South China Sea (Figures S8). On the other hand, coastlines

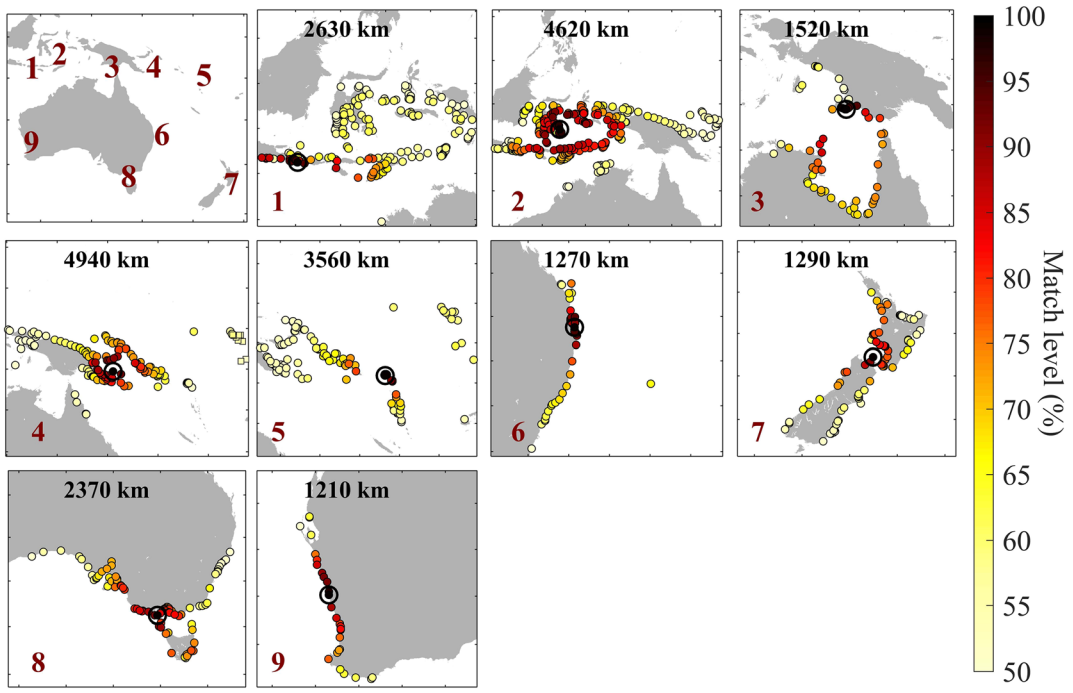

Figure 2. Match level (in percentage) between nine reference series and all other surge series for the Oceania region. Only locations with match levels higher than 50% are displayed. The approximate lengths of the clusters (in kilometers) are indicated in the subplots.

showing less variability of orientation are represented by a relatively smaller number of clusters, as, for example, along the southeastern Pacific (Figures S10), southeastern Atlantic (Figures S9), and Oceania coasts (Figures 2 and 4). Negligible changes are found in the spatial footprints of Oceania and northwestern Atlantic regions when comparing the results obtained by using 95th (Figures 3–6) and 99th percentile thresholds (Figures S37 to S40).

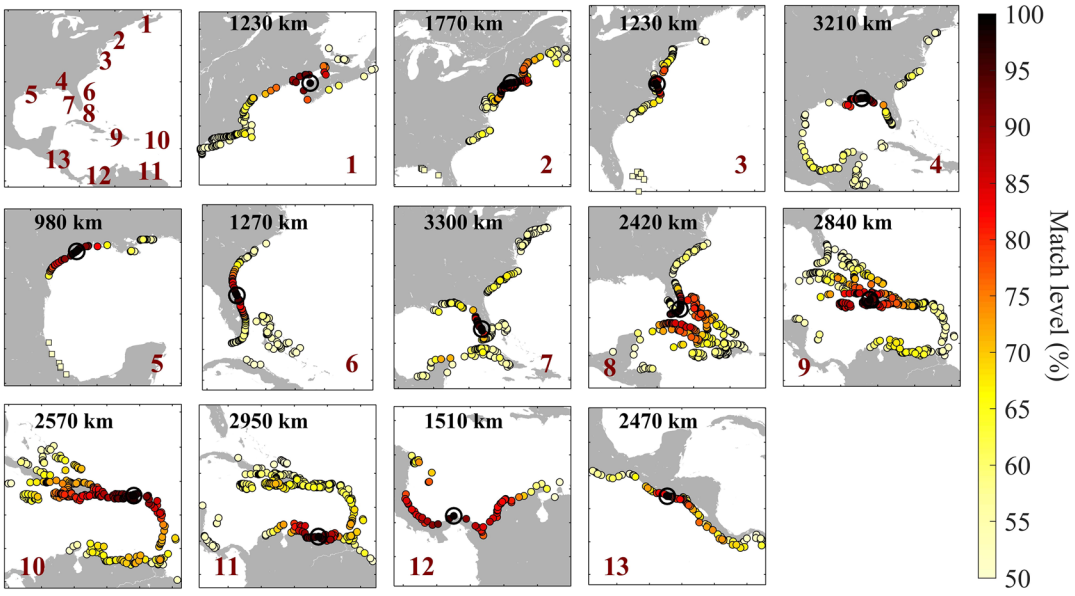

Figure 3. Match level (in percentage) between 13 reference series and all other surge series for the northwestern Atlantic region. Only locations with match levels higher than 50% are displayed. The approximate lengths of the clusters (in kilometers) are indicated in the subplots. Locations indicated by squares indicate the locations excluded in the length calculation.

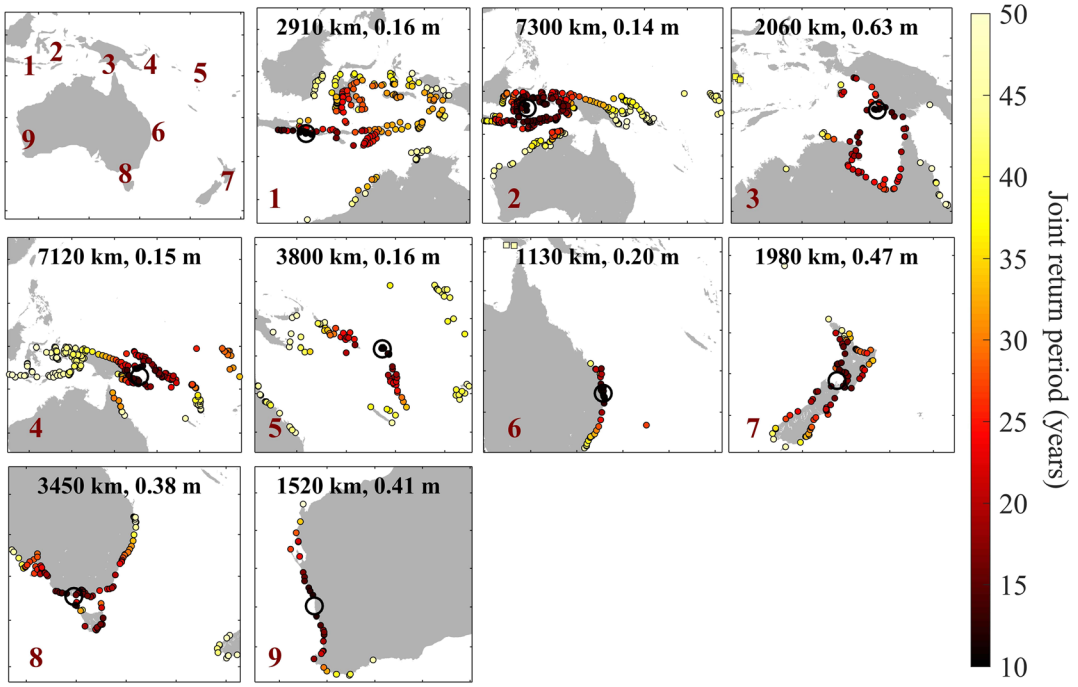

Figure 4. Joint return periods (in years) for the Oceania region between nine reference series and all other surge series for events where the univariate 10-year return levels are exceeded simultaneously. Only locations with joint return periods lower than 50 years are displayed. In addition, the univariate 10-year return levels for each reference surge series (in meters) and the approximate lengths of each cluster (in kilometers) are included in the subplots. Squares indicate the locations excluded in the length calculation because of the spatial disconnect.

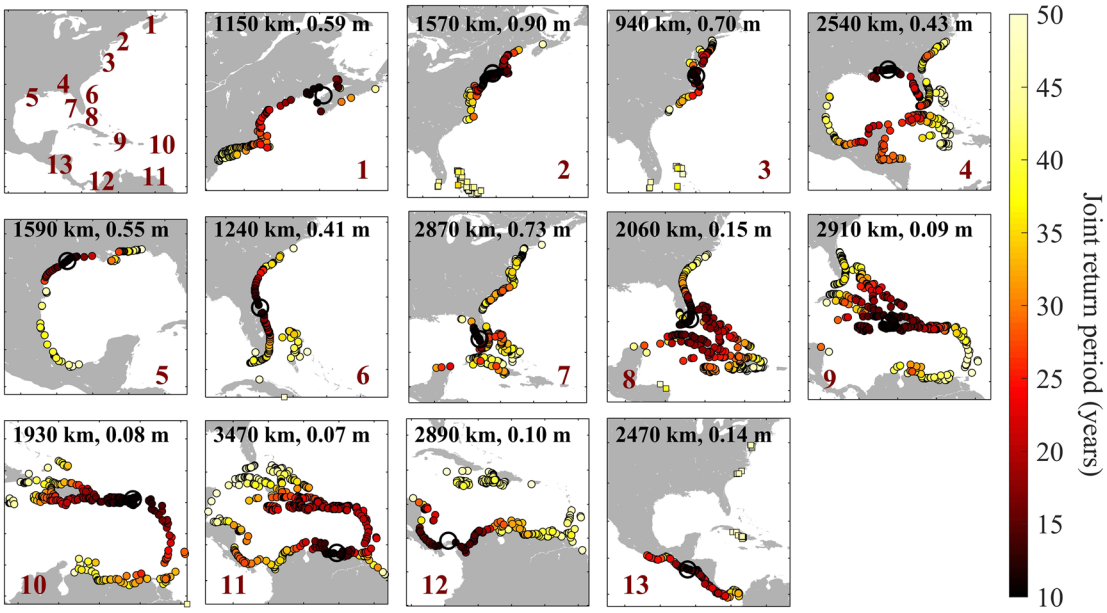

Figure 5. Joint return period (in years) for the northwestern Atlantic region between 13 reference series and all other surge series for events where both univariate 10-year return levels are exceeded simultaneously. Only locations with joint return periods lower than 50 years are displayed. In addition, the univariate 10-year return levels for each reference surge series (in meters) and the approximate length of each cluster (in kilometers) are included in the subplots. Squares indicate the locations excluded in the length calculation.

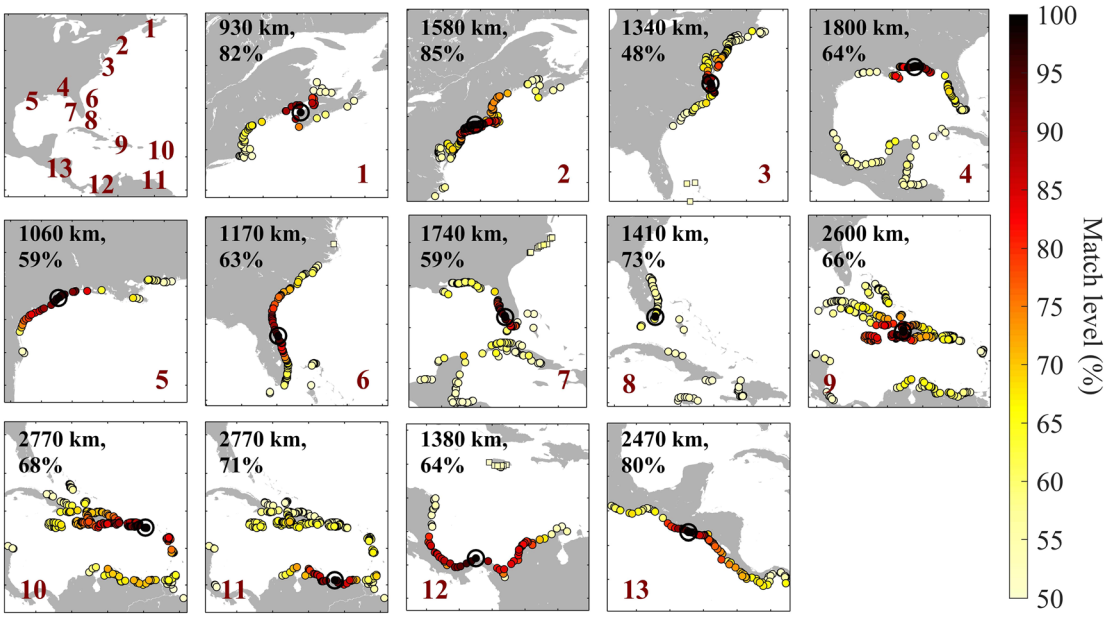

Figure 6. Match level (in percentage) between 13 reference series and all other surge series in the northwestern Atlantic region. Here, simulated surge data specifically account for tropical cyclones. Only locations with match levels higher than 50% are displayed. In addition, the rough length of each cluster (in kilometers) and the percentage of the storm surge time series that are also found in the same spatial footprint when using the first version of GTSR are indicated in the subplots. Locations indicated by squares indicate the locations excluded in the length calculation.

Figures 2 (Oceania coasts) and 3 (northwestern Atlantic coasts) map the match levels between the reference series and all other surge time series. In this case, only storm surge time series showing match levels higher than 50% are shown, thus ensuring that storm surge time series are highly correlated. Spatial footprints showing match levels higher than 70% can be found in Figures S35 and S36. The lengths of these highly correlated coastal stretches are shown in the subplots (units are in kilometer), which are estimated by computing the distances of the locations that are furthest apart. However, those locations entirely separated and unconnected from the main spatial footprint are treated as outliers and thus not considered when computing the lengths of the spatial footprints (the locations excluded in the length calculation are indicated as squares in the figures). As expected, match levels are highest in the areas around the locations where the reference series come from, but there are also many examples of unconnected coastlines belonging to the same clusters, meaning that they are often affected by the same storm surge events, despite their geographic separation, as in the case of the Spatial Footprints 2 and 4 in the northwestern Atlantic region (Figure 3).

Figures 4 (Oceania) and 5 (northwestern Atlantic coasts) map the AND joint return periods corresponding to the probabilities that the univariate 10-year return levels are exceeded simultaneously at the reference location and each of the other locations (paired one-by-one with the reference series in a bivariate copula analysis). Similar to the match level case, we restrict our results in order to show highly correlated spatial footprints; only those locations that have joint return periods of less than 50 years are shown. Note that under the independence assumption, that is, no spatial correlation, the joint return period would be 100 years. The lengths and the univariate 10-year return levels of the reference series (see section 4.3) are indicated in Figures 4 and 5. The same results but for univariate 50-year return levels can be found in Figures S33 and S34; in this case the results are shown for locations with joint return periods of less than 150 (whereas the independent assumption leads to a joint return period of 2,500 years).

We note that some spatial footprints obtained by using copula analysis show spurious dependences between coastal locations that are far way, resulting from fortuitous correlation between two storm surge time series. This is the case, for instance, for the Spatial Footprints 1 and 5 along the northeastern Atlantic coasts (Figure S22). These spurious connections are not evident when using match level analysis (Figure S14). Spurious connections also disappear when applying a higher threshold of match level or joint return period (e.g., the Spatial Footprint 13 in Figure 5 in comparison with the same spatial footprint in Figure S34). However, potentially relevant (for coastal impact assessments) spatial dependences also disappear when

increasing the threshold (from 50% to 70% match level and going from 10- to 50-year univariate return level thresholds and only depicting locations with joint return periods of 150 years or less, which is more restrictive than in the original analysis and removes some weakly correlated pairs).

Match level and joint return period results allow us to identify overlaps between some coastal stretches, despite them being assigned into separate clusters by the K-Means algorithm (Figures S2 and S3). This is particularly noticeable along coastlines of Florida and from Virginia to Massachusetts, northwestern Atlantic region, and northern Oceania.

As expected, the size of the spatial footprints is highly variable and depends on the location and orientation of the coastlines as well as the method employed. For instance, the average spatial footprint length is 2,135 km, varying from 989 to 3,300 km, along the northwestern Atlantic coasts, and 2,600 km on average, varying from 1,210 to 4,940 km, in Oceania when using the match level method. The cluster lengths change when using the copula approach: 2,125 km on average, varying from 940 to 3,470 km, in the northwestern Atlantic and 3,474 km on average, varying from 1,130 to 7,300 km, in the Oceania region.

We perform a sensitivity test to determine the influence of major storm surge events on the extent of the spatial footprints. To do this, we remove the three largest storm surge events in each storm surge time series and repeat the analyses by applying the three methods (K-Means, match level, and copula analysis). The results (Figures S28 to S30) show that the spatial footprints are stable, reflecting the correlated coastlines in terms of extreme storm surges, regardless of the magnitude of (individual) events. The sensitivity test is repeated by using 50-year return levels (Figure S31), finding no differences when removing the three largest events.

4.3. Spatial Footprints of Storm Surges on Northwestern Atlantic Coasts Including Tropical Cyclone Storm Track Information

As mentioned above, the spatial footprints of storm surges on northwestern Atlantic coasts are also assessed by using the updated version of GTSR, which specifically accounts for tropical cyclones. Note that the spatial resolution of this updated reanalysis data set differs from the first version since it does not follow the Dynamic Interactive Vulnerability Assessment segmentation scheme (see section 3). In order to allow a direct comparison, the spatial resolution of the updated reanalysis data set has been adapted by subsampling the model output to match the original GTSR data set. In addition, the same number of clusters and reference stations have been imposed.

Figures 6 and 7 map the match levels and joint return periods, respectively, between the reference series and all other storm surge time series when using the updated version of GTSR. In order to ease the comparison, the percentage of the storm surge time series that are also found in the same spatial footprint when using the first version of GTSR is shown in the figures. The univariate 10-year return levels at the reference locations notably increase (average of 27-cm increase across footprints) when specifically accounting for tropical cyclones (Figure 7). The size of the spatial footprints remains approximately equal when using the copula approach, increasing from 2,125 (Figure 5) to 2,160 km on average (increase of 34 km or 1.6%; Figure 7). However, it decreases from 2,135 (Figure 3) to 1,770 km when using the match level method (decrease of 365 km or 17%, on average; Figure 6) when explicitly accounting for tropical cyclone information, but the overall spatial picture is relatively stable. Note that the spatial footprints obtained from the two methods are not directly comparable, since the match level and copula analysis units are not equivalent; the comparison is between results obtained with the original GTSR and the updated version.

5. Discussion

We use reanalysis and observed storm surge data to identify the spatial footprints of storm surges in 10 regions, covering the world's coastline. The spatial footprints of storm surges obtained by using tide gauge observations and reanalysis data are consistent when the spatial resolution of both data sets is equal (i.e., reanalysis data only used at tide gauge locations) and the same *NoC* is imposed. When *NoC* values are allowed to change the restricted (to tide gauge locations) reanalysis data leads to a larger number of *NoC* in many locations, indicating stronger spatial variability in the model as opposed to what is observed at the tide gauges. As expected, when using the complete reanalysis data set (with much higher spatial resolution), the number of clusters notably increases. This finding stresses that the sparseness of tide gauges is a limiting factor in the assessment of the spatial footprints of storm surges in some regions. While beyond the scope of the

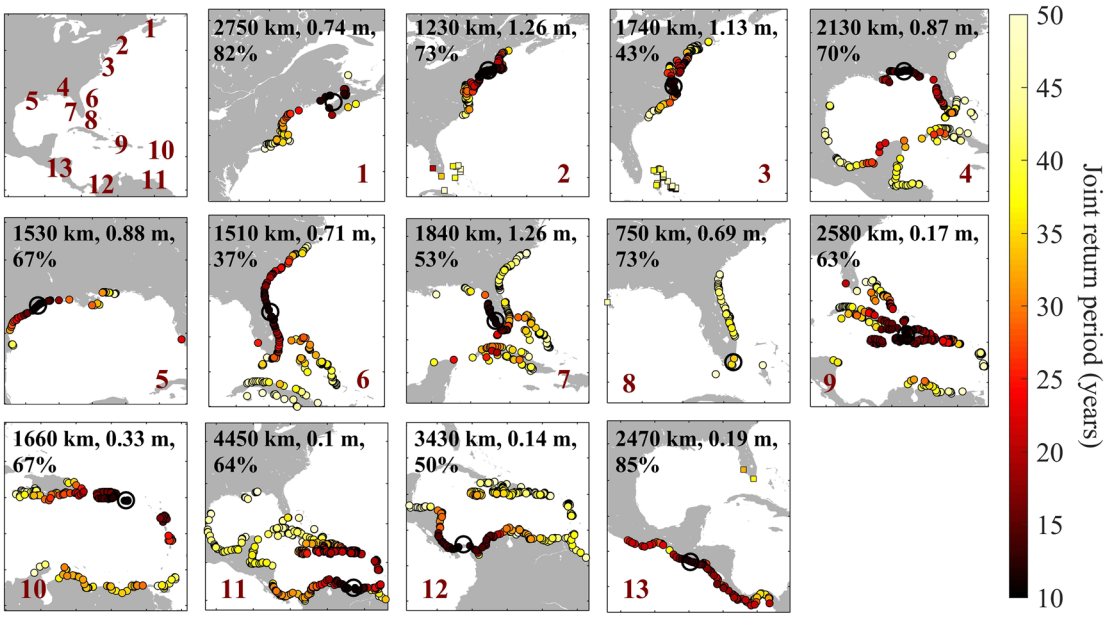

Figure 7. Joint return period (in years) between 13 reference series and all other surge series for 10-year return period in the northwestern Atlantic coasts. Here, simulated surge data specifically account for tropical cyclones. Only those surge series points showing joint return periods lower than 50 years are displayed. In addition, the univariate 10-year return levels calculated for each reference surge series (in meters), the approximate lengths of clusters (in kilometers), and the percentage of the storm surge time series that are also found in the same spatial footprint when using the first version of GTSR are indicated in the subplots. Locations indicated by squares indicate the locations excluded in the length calculation.

present study, further research could include evaluation of the capability of (along-track) altimetry data to validate the spatial footprints of surges. Issues that would have to be addressed in this context include the decline of accuracy of altimetry data near the coast, low temporal resolution, and uncertainties derived from error corrections (Benveniste et al., 2019; Taburet et al., 2019).

Initially, the K-Means algorithm is applied to cluster the storm surge time series according to their correlation and variance. The clustering obtained showed that for coastlines with complex geographies, more clusters are required to represent the spatial footprints of storm surges. In this sense, future work can be devoted to the study of the effects of other factors on the spatial footprint extensions such as storm tracks and sizes. In addition, the K-Means algorithm allows us to obtain the reference series, which represent the storm surge pattern of each cluster.

K-Means clustering, however, does not provide information about the level of similarity among the storm surge time series within each cluster. Thus, the match levels and joint return periods between the reference series and all other storm surge series (regardless of the previous clustering) are also calculated. Match level and joint return period results are defined through more than 50% match and lower than 50-year joint return periods, respectively, thus ensuring correlated coastlines (results for other thresholds can be found in the supporting information, with similar results). As expected, the lengths of correlated coastlines change in comparison with the K-Means clustering. In addition, the match level and joint return period methods allow us to identify overlap between different spatial footprints. Hence, while K-Means clustering is useful for grouping different storm surge time series and identifying the reference series of a region, results should be interpreted with caution when studying closely linked coastlines.

We assess in more detail the storm surge footprints along the northwestern Atlantic coast using an updated reanalysis data set which specifically accounts for tropical cyclone storm track information (Muis et al., 2019). Overall, the spatial picture remains relatively stable, despite the original data set (without storm track information) significantly underestimates the height of many extreme events and hence the associated univariate return levels of the reference series, this is in line with previous studies (Muis et al., 2016, 2019). Future work should include the analysis of spatial footprints from extratropical and tropical events separately, with the known restriction of limited data for tropical cyclone surges when only relying on atmospheric reanalysis (Bloemendaal et al., 2019, 2020).

Spatial footprints of storm surges were studied in previous works. Haigh et al. (2016) used tide gauge data to understand the spatial patterns of extreme sea levels and skew surges along the U.K. coast. They evaluated the spatial footprints by assessing extreme sea level events that impacted at least four tide gauge sites. Despite the regional focus of that work, three out of four spatial footprints of skew surges found in Haigh et al. (2016) (Figure S32) are also reflected in the clusters we obtained for the northeastern Atlantic coast (Figure S14 and S22), for example, the spatial pattern located at the southwestern U.K. coast matches Spatial Footprint 8 of the present study. Haigh et al. (2016) limited their assessment to tide gauges located on the U.K. coast; here, however, we showed that this cluster extends to Ireland and France. The western U.K. spatial pattern found by Haigh et al. (2016) is represented by Spatial Footprint 14, which also extends to the Irish coast. Finally, the southeastern U.K. spatial pattern is reflected by Cluster 5, which extends further along the North Sea coast. The spatial pattern found along the northern U.K. coast by Haigh et al. (2016) is not reflected in any of the clusters identified here.

Following the methodology of Haigh et al. (2016), Stephens et al. (2020) performed a spatial and temporal analysis of extreme sea level and skew surge events around the New Zealand coasts. They found two different spatial patterns of skew surges, whereas our analysis does not point to such spatial differences (Figures 2 and 4). Instead, we find one cluster with its center located at the southern North Island coast, and it extends along the entire coastline of New Zealand.

Although they are not expected to reflect the spatial footprint of specific storm surge events, we note the agreement between some spatial footprints and individual extreme storm surge events, mostly caused by notable named storms. For instance, spatial footprints in northwestern Atlantic coasts (Figures 6 and 7) reflect the spatial track of Tropical Cyclone Irma (Dullaart et al., 2020) in Cluster 7; Hurricanes Harvey (Sebastian et al., 2017), Ike (Muis et al., 2019), and Rita (Dietrich et al., 2010) in Cluster 5; and Tropical Cyclones Michael (Dullaart et al., 2020) and Katrina (Muis et al., 2019) in Cluster 4. Further north, Hurricanes Florence (Dullaart et al., 2020), Ophelia (in 2005, Mattocks & Forbes, 2008), and Irene (Muis et al., 2019) are represented in Cluster 3 and Superstorm Sandy (Muis et al., 2019) in Cluster 2. In the northeastern Atlantic region (Figures S14 and S22), the spatial footprint of the storm surge caused by Extratropical Cyclone Ophelia (in 2017; Dullaart et al., 2020) is represented by Cluster 14. The spatial footprint of Cyclone Xaver (in 2013), which caused extreme storm surges in eastern United Kingdom, Belgium, the Netherlands, Denmark, Germany, and southern Scandinavia (Rucińska, 2019), is reflected in Cluster 5. Our sensitivity analysis (Figures S28 to S30) highlights that the spatial footprints are not biased toward these individual extreme events; instead, it indicates that many other events had similar footprints but were smaller in height and intensity (while still exceeding the 95% or 99% percentile thresholds) and therefore did not cause significant damages. These results would suggest that the spatial footprints of storm surges are conditioned by the storm track direction, but they are less influenced by the intensity. This may change in the future as sea levels continue to rise.

6. Conclusions

In this study we performed the first global analysis of storm surge footprints. We identified the coastal stretches prone to be impacted simultaneously by a storm surge event. Both observed and simulated storm surge data sets were used to describe, quantify, and understand these spatial footprints along the global coastlines by using three different statistical methods: K-Means clustering algorithm, percentage of co-occurrence, and joint probability analysis. Our results showed that not only contiguous but also unconnected coastlines are often affected by the same storm surge events.

Through a validation analysis, we proved the capability of the simulated data to correctly represent the extension of the spatial patterns of storm surges. On the contrary, we found a disagreement in the *NoC* when using observed versus simulated data. The comparison with the spatial footprints obtained from using observed storm surge data allowed us to stress the relevance of the spatial coverage of the data when studying spatial footprints. The clustering obtained from the K-Means algorithm showed the importance of the coastal geography; coastlines with complex geography need a higher number of clusters to represent the spatial footprints of storm surges. Some examples are the Mediterranean, northern European, and South China Sea coasts.

Our results provide a first step toward improving coastal impact assessments. For instance, the K-Means algorithm provided the reference series, which can be employed as indicators of storm surge behavior for spatially coherent coastlines; this set of reference series is an important outcome of the present study. The identification of the coastal regions with spatially coherent footprints can be also employed to improve statistical analysis. In this sense, previous works found a better fit in the extreme value analysis of storm surges when applying a regional approach (in homogenous areas) than the traditional at-site analysis (Bardet et al., 2011; Bernardara et al., 2011). Similar results were shown for other ocean parameters such as waves (Weiss et al., 2014), where uncertainties of return levels were found to be reduced when applying regional frequency analysis. In addition, the knowledge of the dependences among coastal points can be used to simulate statistical storm surge data sets, as previously done for other hazards (Quinn et al., 2019).

Mapping and understanding the spatial footprints of storm surges can help to reduce the impacts of large-scale extreme events, which are exacerbated due to the weakened capacity of the emergency response system, faced with large populations, interconnected infrastructure systems, and multiple industrial sectors being affected simultaneously. The knowledge gained through the spatial footprint analysis presented here (including the identification of the reference series) facilitates improved spatial planning and resource allocation for disaster response, including in areas with sparse sea level observations.

The global approach of the present study allows us to obtain large-scale spatial footprints of storm surges across different regions/states, regardless of national borders. In contrast to studies focused on specific regions, limited by political borders, spatial footprints covering different states highlight the necessity of further collaboration across states to derive effective coastal defense and emergency response plans, especially if the implicated states are economically linked.

Data Availability Statement

Spatial and temporal analysis of extreme sea level and storm surge events around the coastline of the UK. *Scientific Data, 3* (November), 1–23. https://doi.org/10.1038/sdata.2016.107.

Acknowledgments

T. W. and A. R. E. acknowledge support by the National Science Foundation (under Grant ICER-1854896). We thank Sanne Muis for providing surge and extreme sea level reanalysis data from the Global Reanalysis of Storm Surge and Extreme Sea Levels (GTSR) data set (available at https://doi.org/10.4121/uuid:17769b8a-33cd-455c-8bbd-b65ab504f07e) and the Global Extreme Sea Level Analysis (GESLA, available at https://gesla.org/) for making the observed sea level data available. We thank Ivan Haigh for providing Figure S32, previously published in Haigh et al. (2016).

References

Bardet, L., Duluc, C. M., Rebour, V., & L'Her, J. (2011). Regional frequency analysis of extreme storm surges along the French coast. *Natural Hazards and Earth System Science*, *11*(6), 1627–1639. https://doi.org/10.5194/nhess-11-1627-2011

Benveniste, J., Cazenave, A., Vignudelli, S., Fenoglio-Marc, L., Shah, R., Almar, R., et al. (2019). Requirements for a coastal hazards observing system. *Frontiers in Marine Science*, *6*. https://doi.org/10.3389/fmars.2019.00348

Berghuijs, W. R., Allen, S. T., Harrigan, S., & Kirchner, J. W. (2019). Growing spatial scales of synchronous river flooding in Europe. *Geophysical Research Letters*, *46*, 1423–1428. https://doi.org/10.1029/2018GL081883

Bernardara, P., Andreewsky, M., & Benoit, M. (2011). Application of regional frequency analysis to the estimation of extreme storm surges. *Journal of Geophysical Research*, *116*, C02008. https://doi.org/10.1029/2010JC006229

Bloemendaal, N., Haigh, I. D., de Moel, H., Muis, S., Haarsma, R. J., & Aerts, J. C. J. H. (2020). Generation of a global synthetic tropical cyclone hazard dataset using STORM. *Scientific Data*, *7*(1), 40–12. https://doi.org/10.1038/s41597-020-0381-2

Bloemendaal, N., Muis, S., Haarsma, R. J., Verlaan, M., Irazoqui Apecechea, M., de Moel, H., et al. (2019). Global modeling of tropical cyclone storm surges using high-resolution forecasts. *Climate Dynamics*, *52*(7–8), 5031–5044. https://doi.org/10.1007/s00382-018-4430-x

Church, J. A., & White, N. J. (2006). A 20th century acceleration in global sea-level rise. *Geophysical Research Letters*, *33*, L01602. https://doi.org/10.1029/2005GL024826

Dietrich, J. C., Bunya, S., Westerink, J. J., Ebersole, B. A., Smith, J. M., Atkinson, J. H., et al. (2010). A high-resolution coupled riverine flow, tide, wind, wind wave, and storm surge model for southern Louisiana and Mississippi. Part II: Synoptic description and analysis of Hurricanes Katrina and Rita. *Monthly Weather Review*, *138*(2), 378–404. https://doi.org/10.1175/2009MWR2907.1

Dullaart, J. C. M., Muis, S., Bloemendaal, N., & Aerts, J. C. J. H. (2020). Advancing global storm surge modelling using the new ERA5 climate reanalysis. *Climate Dynamics*, *54*(1-2), 1007–1021. https://doi.org/10.1007/s00382-019-05044-0

Haigh, I. D., Wadey, M. P., Wahl, T., Ozsoy, O., Nicholls, R. J., Brown, J. M., et al. (2016). Spatial and temporal analysis of extreme sea level and storm surge events around the coastline of the UK. *Scientific Data*, *3*(1), 160,107–160,123. https://doi.org/10.1038/sdata.2016.107

Hallegatte, S., Green, C., Nicholls, R. J., & Corfee-Morlot, J. (2013). Future flood losses in major coastal cities. *Nature Climate Change*, *3*(9), 802–806. https://doi.org/10.1038/nclimate1979

Hastie, T., Tibshirani, R., & Friedman, J. (2009). *The elements of statistical learning: data mining, inference, and prediction* (Vol. 2). New York, NY: Springer Science & Business Media. https://doi.org/10.1007/b94608

Hope, M. E., Westerink, J. J., Kennedy, A. B., Kerr, P. C., Dietrich, J. C., Dawson, C., et al. (2013). Hindcast and validation of Hurricane Ike (2008) waves, forerunner, and storm surge scale concave geometry generated waves and surge that impacted over 1000 km of coastline. *Ike's Complex and Varied Wave and Surge Response Physics Included: The Cap*, *118*(9), 4424–4460. https://doi.org/10.1002/jgrc.20314

Jongman, B., Hochrainer-Stigler, S., Feyen, L., Aerts, J. C. J. H., Mechler, R., Botzen, W. J. W., et al. (2014). Increasing stress on disaster-risk finance due to large floods. *Nature Climate Change*, *4*(4), 264–268. https://doi.org/10.1038/nclimate2124

Keef, C., Svensson, C., & Tawn, J. A. (2009). Spatial dependence in extreme river flows and precipitation for Great Britain. *Journal of Hydrology*, *378*(3–4), 240–252. https://doi.org/10.1016/j.jhydrol.2009.09.026

Marcos, M., & Woodworth, P. L. (2017). Spatiotemporal changes in extreme sea levels along the coasts of the North Atlantic and the Gulf of Mexico. *Journal of Geophysical Research: Oceans*, *122*, 7031–7048. https://doi.org/10.1002/2017JC013065

Mattocks, C., & Forbes, C. (2008). A real-time, event-triggered storm surge forecasting system for the state of North Carolina. *Ocean Modelling*, *25*(3-4), 95–119. https://doi.org/10.1016/j.ocemod.2008.06.008

Mawdsley, R. J., Haigh, I. D., & Wells, N. C. (2015). Global secular changes in different tidal high water, low water and range levels. *Earth's Future*, *3*(2), 66–81. https://doi.org/10.1002/2014EF000282

McGranahan, G., Balk, D., & Anderson, B. (2007). The rising tide: Assessing the risks of climate change and human settlements in low elevation coastal zones. *Environment and Urbanization*, *19*(1), 17–37. https://doi.org/10.1177/0956247807076960

Muis, S., Lin, N., Verlaan, M., Winsemius, H. C., Ward, P. J., & Aerts, J. C. J. H. (2019). Spatiotemporal patterns of extreme sea levels along the western North-Atlantic coasts. *Scientific Reports*, *9*(1), 1–12.

Muis, S., Verlaan, M., Winsemius, H. C., Aerts, J. C. J. H., & Ward, P. J. (2016). A global reanalysis of storm surges and extreme sea levels. *Nature Communications*, *7*(1), 11969. https://doi.org/10.1038/ncomms11969

Needham, H. F., Keim, B. D., & Sathiaraj, D. (2015). A review of tropical cyclone-generated storm surges: Global data sources, observations, and impacts. *Reviews of Geophysics*, *53*, 545–591. https://doi.org/10.1002/2014RG000477

Neumann, B., Vafeidis, A. T., Zimmermann, J., & Nicholls, R. J. (2015). Future coastal population growth and exposure to sea-level rise and coastal flooding—A global assessment. *PloS One*, *10*(3), e0118571. https://doi.org/10.1371/journal.pone.0118571

NWS, N. H. C (2019a). Hurricane Dorian Advisory Number 33. Miami, Florida. Retrieved from https://www.nhc.noaa.gov/archive/2019/al05/al052019.public.033.shtml

NWS, N. H. C. (2019b). Hurricane Dorian Intermediate Advisory Number 51A. Miami, Florida. Retrieved from https://www.nhc.noaa.gov/archive/2019/al05/al052019.public_a.051.shtml

Quinn, N., Bates, P. D., Neal, J., Smith, A., Wing, O., Sampson, C., et al. (2019). The spatial dependence of flood hazard and risk in the United States. *Water Resources Research*, *55*, 1890–1911. https://doi.org/10.1029/2018WR024205

Rego, J. L., & Li, C. (2010). Storm surge propagation in Galveston Bay during Hurricane Ike. *Journal of Marine Systems*, *82*(4), 265–279. https://doi.org/10.1016/j.jmarsys.2010.06.001

Rucińska, D. (2019). Describing Storm Xaver in disaster terms. *International Journal of Disaster Risk Reduction*, *34*, 147–153. https://doi.org/10.1016/j.ijdrr.2018.11.012

Salvadori, G., & De Michele, C. (2004). Frequency analysis via copulas: Theoretical aspects and applications to hydrological events. *Water Resources Research.*, *40*, W12511. https://doi.org/10.1029/2004WR003133

Sebastian, A. G., Lendering, K. T., Kothuis, B. L. M., Brand, A. D., Jonkman, S. N., van Gelder, P., et al. (2017). Hurricane Harvey Report: A fact-finding effort in the direct aftermath of Hurricane Harvey in the Greater Houston Region. https://www.researchgate.net/publication/321749153_Hurricane_Harvey_Report_A_fact-finding_effort_in_the_direct_aftermath_of_Hurricane_Harvey_in_the_Greater_Houston_Region

Stephens, S. A., Bell, R. G., & Haigh, I. (2020). Spatial and temporal analysis of extreme storm-tide and skew-surge events around the coastline of New Zealand. *Natural Hazards and Earth System Sciences*, *20*(3), 783–796.

Taburet, G., Sanchez-Roman, A., Ballarotta, M., Pujol, M. I., Legeais, J. F., Fournier, F., et al. (2019). DUACS DT2018: 25 years of reprocessed sea level altimetry products. *Ocean Science*, *15*(5), 1207–1224. https://doi.org/10.5194/os-15-1207-2019

Vafeidis, A. T., Nicholls, R. J., McFadden, L., Tol, R. S. J., Hinkel, J., Spencer, T., et al. (2008). A new global coastal database for impact and vulnerability analysis to sea-level rise. *Journal of Coastal Research*, *244*, 917–924. https://doi.org/10.2112/06-0725.1

Villarini, G., Smith, J. A., Baeck, M. L., Marchok, T., & Vecchi, G. A. (2011). Characterization of rainfall distribution and flooding associated with U.S. landfalling tropical cyclones: Analyses of Hurricanes Frances, Ivan, and Jeanne (2004). *Journal of Geophysical Research*, *116*, D23116. https://doi.org/10.1029/2011JD016175

Von Storch, H., & Woth, K. (2008). Storm surges: Perspectives and options. *Sustainability Science*, *3*(1), 33–43. https://doi.org/10.1007/s11625-008-0044-2

Vousdoukas, M. I., Mentaschi, L., Hinkel, J., Ward, P. J., Mongelli, I., Ciscar, J. C., & Feyen, L. (2020). Economic motivation for raising coastal flood defenses in Europe. *Nature Communications*, *11*(1), 2119–2111. https://doi.org/10.1038/s41467-020-15665-3

Vousdoukas, M. I., Mentaschi, L., Voukouvalas, E., Verlaan, M., Jevrejeva, S., Jackson, L. P., & Feyen, L. (2018). Global probabilistic projections of extreme sea levels show intensification of coastal flood hazard. *Nature Communications*, *9*(1), 2360–2312. https://doi.org/10.1038/s41467-018-04692-w

Wahl, T., & Chambers, D. P. (2015). Evidence for multidecadal variability in US extreme sea level records. *Journal of Geophysical Research: Oceans*, *120*, 1527–1544. https://doi.org/10.1002/2014JC010443

Wahl, T., & Chambers, D. P. (2016). Climate controls multidecadal variability in US extreme sea level records. *Journal of Geophysical Research: Oceans*, *121*, 1274–1290. https://doi.org/10.1002/2015JC011057

Wahl, T., Haigh, I. D., Nicholls, R. J., Arns, A., Dangendorf, S., Hinkel, J., & Slangen, A. B. A. (2017). Understanding extreme sea levels for broad-scale coastal impact and adaptation analysis. *Nature Communications*, *8*(1), 16075. https://doi.org/10.1038/ncomms16075

Wahl, T., Jain, S., Bender, J., Meyers, S. D., & Luther, M. E. (2015). Increasing risk of compound flooding from storm surge and rainfall for major US cities. *Nature Climate Change*, *5*(12), 1093–1097. https://doi.org/10.1038/nclimate2736

Wahl, T., Mudersbach, C., & Jensen, J. (2012). Assessing the hydrodynamic boundary conditions for risk analyses in coastal areas: A multivariate statistical approach based on copula functions. *Natural Hazards and Earth System Science*, *12*, 495–510. https://doi.org/10.5194/nhess-12-495-2012

Weiss, J., Bernardara, P., & Benoit, M. (2014). Formation of homogeneous regions for regional frequency analysis of extreme significant wave heights. *Journal of Geophysical Research: Oceans*, *119*, 2906–2922. https://doi.org/10.1002/2013JC009668

Westerink, J. J., Luettich, R. A., Feyen, J. C., Atkinson, J. H., Dawson, C., Roberts, H. J., et al. (2008). A basin-to channel-scale unstructured grid hurricane storm surge model applied to southern Louisiana. *Monthly Weather Review*, *136*(3), 833–864. https://doi.org/10.1175/2007MWR1946.1

Willner, S. N., Otto, C., & Levermann, A. (2018). Global economic response to river floods. *Nature Climate Change*, *8*(7), 594–598. https://doi.org/10.1038/s41558-018-0173-2

Woodworth, P. L., Hunter, J. R., Marcos, M., Caldwell, P., Menéndez, M., & Haigh, I. (2016). Towards a global higher-frequency sea level dataset. *Geoscience Data Journal*, *3*(2), 50–59. https://doi.org/10.1002/gdj3.42